NANO LETTERS
Cite This: Nano Lett. XXXX, XXX, XXX−XXX
Letter
pubs.acs.org/NanoLett

A Two-Dimensional MoS_2 Catalysis Transistor by Solid-State Ion Gating Manipulation and Adjustment (SIGMA)

Yecun Wu,[†,○] Stefan Ringe,[‡,§,○] Chun-Lan Wu,[∥] Wei Chen,[∥] Ankun Yang,[∥] Hao Chen,[∥] Michael Tang,[‡,§] Guangmin Zhou,[∥] Harold Y. Hwang,[⊥,#] Karen Chan,*[,▽] and Yi Cui*[,∥,#]

[†]Department of Electrical Engineering, Stanford University, Stanford, California 94305, United States
[‡]SUNCAT Center for Interface Science and Catalysis, Stanford University, Stanford, California 94305, United States
[§]SUNCAT Center for Interface Science and Catalysis, SLAC National Accelerator Laboratory, Menlo Park, California 94025, United States
[∥]Department of Materials Science and Engineering, Stanford University, Stanford, California 94305, United States
[⊥]Department of Applied Physics, Stanford University, Stanford, California 94305, United States
[#]Stanford Institute for Materials and Energy Science, SLAC National Accelerator Laboratory, Menlo Park, California 94025 United States
[▽]CatTheory Center, Department of Physics, Technical University of Denmark, Kongens Lyngby 2800, Denmark

Supporting Information

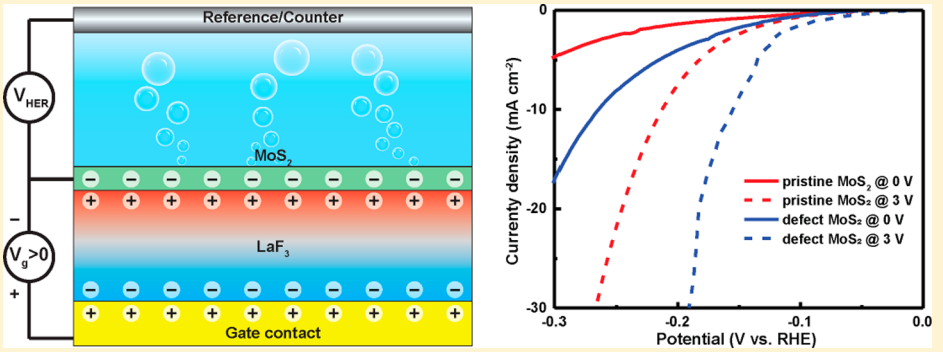

ABSTRACT: A variety of methods including tuning chemical compositions, structures, crystallinity, defects and strain, and electrochemical intercalation have been demonstrated to enhance the catalytic activity. However, none of these tuning methods provide direct dynamical control during catalytic reactions. Here we propose a new method to tune the activity of catalysts through solid-state ion gating manipulation and adjustment (SIGMA) using a catalysis transistor. SIGMA can electrostatically dope the surface of catalysts with a high electron concentration over 5×10^{13} cm^{-2} and thus modulate both the chemical potential of the reaction intermediates and their electrical conductivity. The hydrogen evolution reaction (HER) on both pristine and defective MoS_2 were investigated as model reactions. Our theoretical and experimental results show that the overpotential at 10 mA/cm^2 and Tafel slope can be in situ, continuously, dynamically, and reversibly tuned over 100 mV and around 100 mV/dec, respectively.

KEYWORDS: *Catalysis transistor, solid-state ion gating, electrocatalysis, two-dimensional materials*

Electrocatalysis plays an important role in the conversion of earth-abundant and low-cost resources (H_2O, CO_2, etc.) to high-value products (H_2, CH_4, etc.), especially when coupled with renewable energy.[1] To achieve the goal of highly efficient energy conversion at a low cost, different strategies have been proposed to tune and enhance the catalytic performance of electrocatalysts. The most general methodology is to change the chemical compositions and structure of catalysts to tune the energetics of the reaction intermediates involved.[2−4] Tuning the surface morphology, such as the dominant surface facet, the crystallinity, or the amount of defects in the catalyst is another popular way to improve the electrochemical conversion performance.[5−7] A lithium electrochemical intercalation tuning approach was developed to optimize the activity by varying the electron structure of existing materials.[8] Straining the catalysts through volume expansion/contraction is another effective technique to tune the catalytic performance in a continuous manner.[9,10] Despite the exciting progress, none of these strategies allows for in situ dynamic control over the activity during the reactions. Here,

Received: July 15, 2019
Revised: August 25, 2019
Published: September 9, 2019

Downloaded via STANFORD UNIV on September 16, 2019 at 15:52:59 (UTC).
See https://pubs.acs.org/sharingguidelines for options on how to legitimately share published articles.

© XXXX American Chemical Society

DOI: 10.1021/acs.nanolett.9b02888
Nano Lett. XXXX, XXX, XXX−XXX

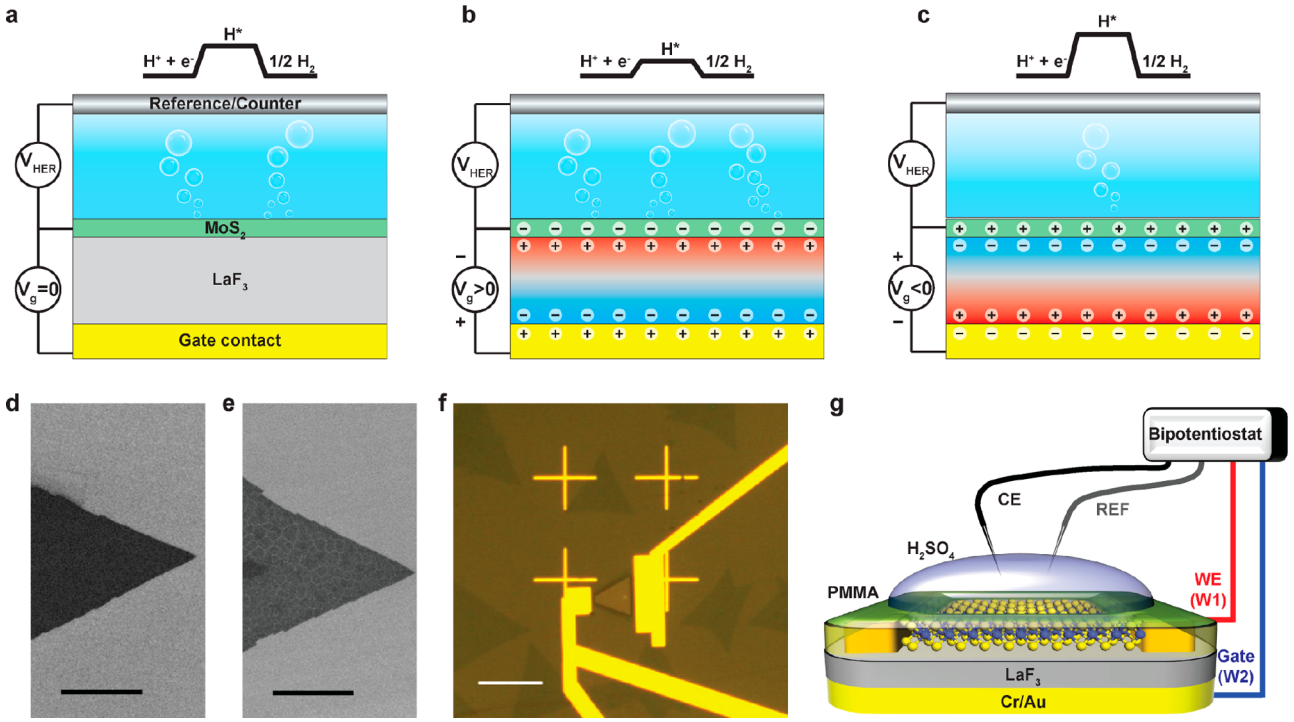

Figure 1. SIGMA for hydrogen evolution reaction. (a) Schematic illustration of the SIGMA approach and HER at zero gate voltage. SIGMA is applied to the bottom of the MoS_2 and HER occurs on the top of MoS_2. The free energy versus the reaction coordinate of HER for MoS_2 is illustrated on top. (b) A positive gate voltage dopes the MoS_2 with electrons, which enhances conductivity of MoS_2 and reduces the hydrogen adsorption energy, thus enhancing the catalytic performance. (c) A negative gate voltage dopes the MoS_2 with holes, thus increases the hydrogen adsorption energy. (d) SEM image of CVD grown monolayer pristine MoS_2 (scale bar: 10 μm). (e) SEM image of defective CVD grown MoS_2 generated by Ar plasma etching (scale bar: 10 μm). (f) Optical microscope image of the microcell, where the edge of the MoS_2 is covered by PMMA and the basal plane is exposed for HER (scale bar: 50 μm). (g) Schematic illustration of the experimental setup: a drop of 0.5 M H_2SO_4 is placed on top of the microcell for HER; a bipotentiostat is used to form a three-electrode electrochemical measurement and gate control.

we demonstrate that solid-state ion gating manipulation and adjustment (SIGMA) as an effective method to realize an in situ, dynamic, continuous, and reversible tuning of catalytic activity. SIGMA can manipulate the carrier density of the catalyst, which allows us to optimize the reaction intermediate binding energy and the electrical conductivity to obtain a high-performance catalyst.

Electrostatic gating has been widely used for decades for cutting-edge electronics and photonics[11−13] and extended to a variety of applications.[14−16] However, the relatively small capacitance of traditional gate dielectrics (for example, $\sim 10^{-2}$ μF cm^{-2} for 300 nm SiO_2) results in only a low doping concentration ($\sim 10^{12}$ cm^{-2}) even at high gate voltage (>50 V). Reducing the thickness of dielectrics and increasing the dielectric constant are a direction to improve, but there is a limit due to the leakage current. The electric-double-layer transistor (EDLT) with ionic liquid electrolyte offered over 2 orders of magnitude higher capacitance coupling (~ 7 μF cm^{-2}) and has been successfully used in field effect transistors for accumulating carriers over 10^{14} cm^{-2}.[17] However, it is difficult to apply ionic liquid EDLT to tune electrochemical reactions, especially for liquid phase reactions because there would be a mixing compatibility issue between the reactant electrolyte and ionic gating liquid.

Recently, we have developed a solid-state ion gating method with a similar capacitive coupling strength (~ 4 μF cm^{-2}) as the ionic liquid to induce an insulator−metal transition in MoS_2 transistors by mobile fluoride (F^-) ions in LaF_3.[18] Here we exploit F^- ion solid-ion gating for the first time as the basis of SIGMA for catalyst tuning, which not only maintains high capacitance coupling but also removes the problem of incompatibility of liquid electrolyte mixing. Figure 1a shows our basic device structure, which can be considered as two types of devices stacked together. The top half is an electrocatalytic cell, where a thin layer MoS_2 for hydrogen evolution reaction and a counter electrode for oxygen evolution reaction are in contact with aqueous electrolyte. The bottom half is a solid ion EDL transistor, where the same MoS_2 layer and the gate electrode are coupled through the LaF_3 solid ion conductor. When applying a positive gate voltage in the bottom cell (Figure 1b), the F^- ions migrate and accumulate close to the bottom gate contact by electrostatic attraction, resulting in fluoride vacancies (positive charge) at the upper surface of the LaF_3. The MoS_2 layer on top of the LaF_3 would be negatively doped (n-doped) to balance the charge (Figure 1b). A negative gate voltage generates the opposite effect (Figure 1c). By using this method, the MoS_2 layer can be electron-doped with a concentration of 5×10^{13} cm^{-2} when applying a gate voltage of +3 V.[18] We hypothesize that such a strong gate coupling in this new SIGMA method not only changes the conductivity of catalysts but also modulates the chemical potential of the reaction intermediates (as shown schematically in free energy diagrams in the top part of Figure 1a−c), resulting in significant catalytic activity tuning (shown in our joint theoretical and experimental study below).[7,19]

To demonstrate the SIGMA methodology, we select the MoS_2 catalyzed hydrogen evolution reaction (HER) as a

DOI: 10.1021/acs.nanolett.9b02888
Nano Lett. XXXX, XXX, XXX−XXX

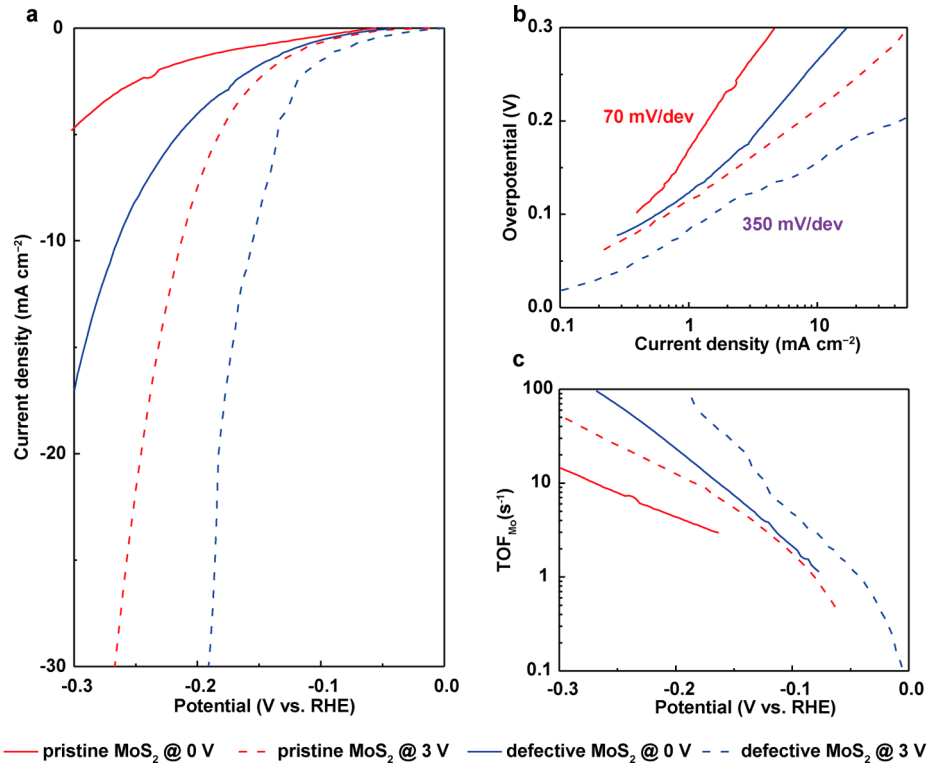

Figure 2. Electrochemical tuning of the MoS_2 HER by SIGMA. (a) Polarization curves measured from the pristine (red) and defective (blue) MoS_2 device at 0 V (solid) and 3 V (dash) gate voltage without *iR* correction. (b) The corresponding Tafel plots of the polarization curves. (c) Corresponding TOF_{Mo} plots of the LSV curves.

model system. In recent years, due to its catalytic activity, low-cost, and earth-abundance, two-dimensional MoS_2 has been regarded as an alternative HER catalyst material to precious metals.[20,21] Additionally, the low out-of-plane and high in-plane dielectric constant of the ultrathin layer make two-dimensional MoS_2 highly desirable for well-controlled electrostatics.[22] However, the inert basal plane and the high electronic resistance of 2H-MoS_2 greatly limit their catalytic performance.[23,24] Intensive studies have been carried out to increase the density of active sites,[25] showing that the HER performance of MoS_2 can be improved by exposing more edges,[26,27] introducing dopants,[3,28,29] or creating sulfur vacancies (defective MoS_2) as active sites.[6,7,30]

In what follows, we show that the HER catalytic activity of both pristine and defective MoS_2 devices can be tuned by SIGMA. We find that SIGMA can dynamically, continuously, and reversibly tune the hydrogen adsorption free energy (ΔG_{ads}) and the conductivity of MoS_2, thus tuning the performance of a catalyst. The overpotential at 10 mA/cm^2 can be decreased by over 100 mV in both pristine and defective MoS_2. SIGMA opens up a new way to dynamically tune the catalytic conversion efficiency independently of the applied potential and without direct modification of the catalyst material or morphology.

Results and Discussions. To investigate the gate effect on the HER of a single layer MoS_2 crystal, we first grew the triangular monolayer MoS_2 by chemical vapor deposition (CVD) on a silicon substrate with 300 nm oxide layer as shown in Figure S1. The defective MoS_2 was fabricated by using mild argon plasma etch of the pristine MoS_2. The SEM images of the pristine and defective MoS_2 are shown in Figure 1d,e. Defective MoS_2 shows short and isolated cracks with a connection angle of ~120°, which is consistent with the previous report.[6] Raman spectra, photoluminescence (PL), and atomic force microscope (AFM) measurements were used to confirm the formation of single layer MoS_2 (Figures S2 and S3). X-ray photoelectron spectroscopy (XPS) was employed to measure the ratio of Mo and S, which is used to determine the density of sulfur vacancies (Figure S4). The Mo and S ratio of the defective samples is 1:1.75 (±0.05), indicating that the sulfur vacancy density is ~12.5% (±3%) (Figure S4). We then transferred the as-grown and plasma-treated samples to a LaF_3 substrate by the polymer-assisted wet transfer method. After the transfer, the sample was annealed in argon atmosphere at 250 °C to remove the contaminants and achieve a high quality LaF_3−MoS_2 contact interface. Subsequently, electron-beam lithography and metal evaporation were used to define and deposit 5 nm of chromium as an adhesion layer and 45 nm gold electrodes as current collectors near the materials. To achieve a low contact resistance, we also fabricated a 50 nm pure Au electrode as a connection between the MoS_2 flake and Cr/Au electrodes. Finally, a layer of 5/50 nm Cr/Au was deposited by e-beam evaporation on the back side of the LaF_3 to form a back-gate structure. The schematic of a MoS_2 solid-state EDL transistor is shown in Figure S5a.

To investigate the electron transport properties in pristine and defective MoS_2, we first performed electrical characterization of our EDL transistors. All the transistors are fabricated with the same channel length and width, and the measurements were performed at room temperature using a semiconductor parameter analyzer with a shielded probe station. The voltage sources connected in the configuration are depicted in the Figure S5a. A 2 V constant source-drain voltage was applied and the bottom ionic gate voltage was

DOI: 10.1021/acs.nanolett.9b02888
Nano Lett. XXXX, XXX, XXX−XXX

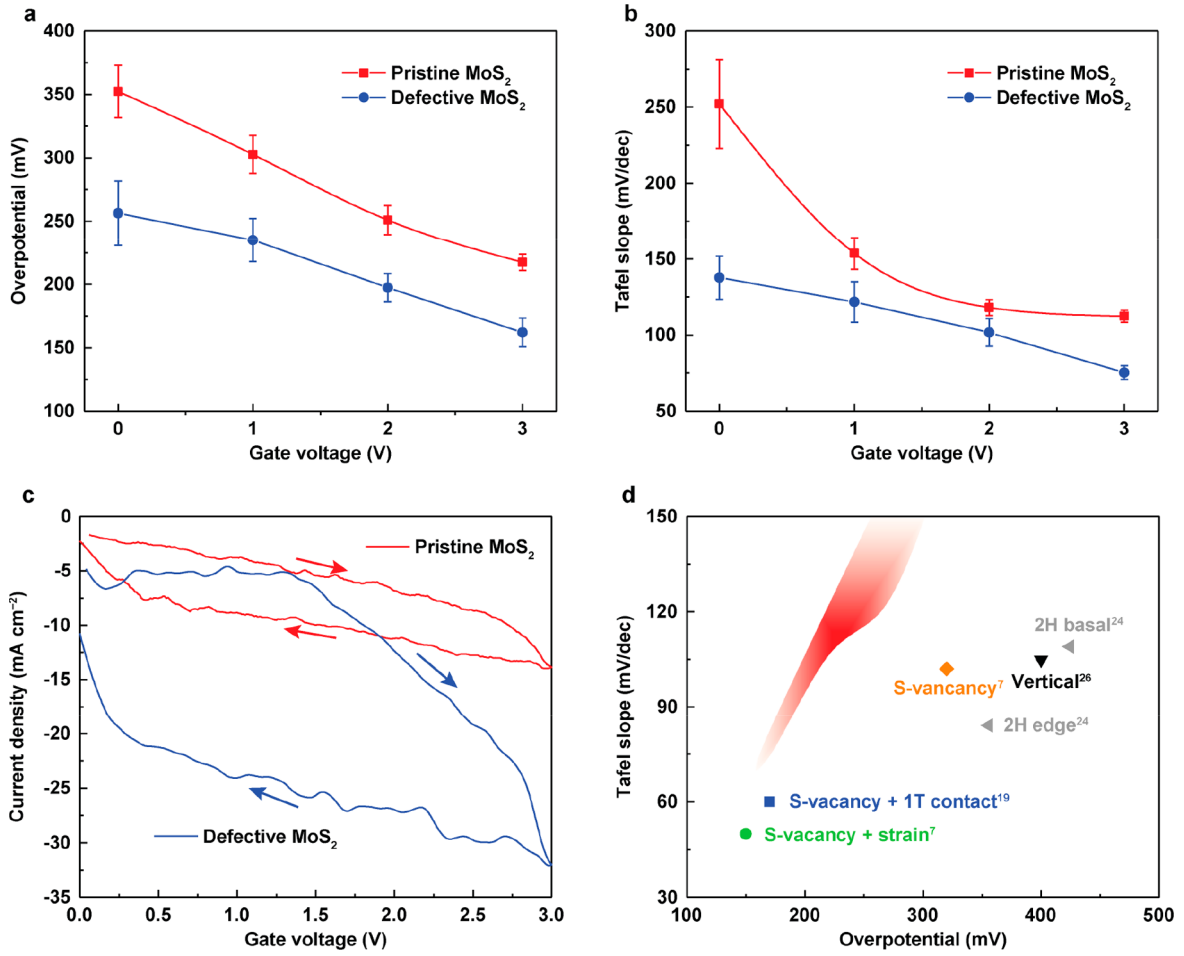

Figure 3. Gate tunable HER performance. (a) The variation of the overpotential at 10 mV/cm^2 with gate voltage. (b) The variation of the Tafel slope with gate voltage. (c) The $I_{HER}-V_g$ transfer curves with $V_{HER} = -0.2$ V. (d) A comparison of the HER performances of CVD MoS_2 modified by different methods. The boundary of the red area is the performance of pristine and defective MoS_2 obtained from (a,b).

swept from −1 to 3 V with 10 mV/s step, while the source-drain current was measured. The gating responses of MoS_2 and defective MoS_2 channel are presented in Figure S5b. Repeated sweeps on the same device did not show significant variation and the leakage is lower than 20 nA. The pristine MoS_2 device demonstrates a typical n-type channel with a threshold voltage and on/off ratio over 10^4. The source-drain current shows a tendency of saturation when the gate voltage is greater than 2.5 V. The carrier density of the EDL transistor can be estimated by using $n = (C \times V)/q$, where the C is the capacitance of the solid-state MoS_2−LaF_3 electrical double layer (~4 μF/cm^2),[18] V is the gate voltage, and q is the charge of an electron (1.6×10^{-19} C). At 3 V gate voltage, the carrier density is estimated to be over 5×10^{13} cm^{-2}. As for the defective MoS_2 channel, limited charge transport was observed. A higher threshold voltage was obtained, and the current at 0 V gate voltage is about one order magnitude lower than that of the pristine MoS_2 channel. This charge transport limit in the subthreshold regime origins from the trap states induced by the defects in the band gap of MoS_2.[31] Despite the current decline at 0 V, the current at higher electron doping concentration is higher than that of the pristine MoS_2 channel device. The in situ Raman spectra of the gate-dependent defective MoS_2 were conducted to confirm that there is no 2H to 1T phase transition at higher gate bias (Figure S6).

To combine the EDL transistor and electrochemical catalysis, a layer of poly(methyl methacrylate) (PMMA) resist is spin-coated as a protection layer (~200 nm) on top of the transistor. A window is then opened in the PMMA by electron beam lithography to cover the edge and expose the basal plane of MoS_2 for HER as shown in the optical microscope image in Figure 1f. A small amount (~30 μL) of the 0.5 M sulfuric acid (H_2SO_4) electrolyte was dropped on top of the device. An Ag/AgCl reference electrode and a sharp carbon rod counter electrode were immersed in the electrolyte to form a three-electrode system. The experiment was performed on a bipotentiostat as shown in Figure 1g. The equivalent circuit can be found in Figure S7. We also used the 0.5 M H_2SO_4 electrolyte as a top gate of the device to confirm that the MoS_2 cannot be gated by the HER electrolyte. The results showed negligible changes of the conductivity of MoS_2 with the top 0.5 M H_2SO_4 gate (Figure S8).

Linear sweep voltammograms (LSV) were performed on both pristine MoS_2 and defective MoS_2 with different gate voltages ranging from 0 to 3 V. The polarized curves of samples at 0 and 3 V gate voltages without *iR* correction in are shown in Figure 2a. The corresponding Tafel slope curves are presented in Figure 2b. Completely polarized curves from 0 to 3 V gate voltage with 1 V steps are shown in the Figure S9. Electrocatalysis from monolayer single crystal MoS_2 also allows an accurate measurement of the surface exposed to the

DOI: 10.1021/acs.nanolett.9b02888
Nano Lett. XXXX, XXX, XXX−XXX

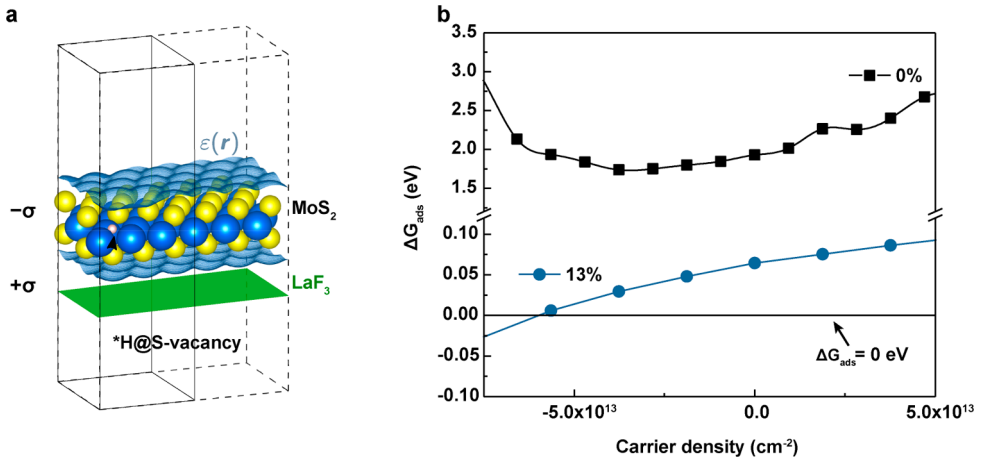

Figure 4. Computational modeling of HER at the MoS_2 sheet under influence of SIGMA. (a) Schematic system setup consisting of MoS_2 sheet embedded into a dielectric continuum that contains a counter charge representing the LaF_3−MoS_2 capacitor. (b) Effect of electron (negative) and hole (positive) carrier density on the adsorption energy of H* for 0% sulfur vacancy and 13% sulfur vacancy at a hydrogen coverage of 16.7% (all S-vacancies occupied with H atoms).

electrolyte, which can be used to calculate the turnover frequency (TOF), an indicator of the activity per single catalytic site. The TOFs of each individual S atom are calculated and shown in Figure 2c to compare the intrinsic activity of different MoS_2 samples. To investigate the correlation between the HER catalytic performance and gate voltage, we fabricated multiple devices and measured the catalytic performance at different gate voltages to obtain statistical data.

The variation of the overpotential at 10 mA/cm^2 and the Tafel slopes of both pristine MoS_2 and defective MoS_2 with different gate voltages are summarized in Figure 3a,b, respectively. For the pristine MoS_2 device, the catalyst shows an overpotential over 300 mV at 10 mA/cm^2 and a Tafel slope over 250 mV/dec at zero gate voltage. As the gate voltage increases to 3 V, this situation is dramatically improved with the overpotential at 10 mA/cm^2 reduced to ∼210 mV. At 3 V gate voltage, the Tafel slope is reduced to 110 mV/dec which has been associated with a Volmer−Heyrovsky mechanism with the adsorption Volmer step ($H^+ + e^- + * \rightarrow H^*$) being the rate-limiting step.[26] The decrease in Tafel slope with gate voltage could be rationalized from the gate-induced electron injection into the *H@MoS_2 system. From our density functional theory (DFT) calculations and Bader charge partitioning analysis,[32] we found this to also negatively charge up the adsorbed *H atoms. We postulate here that this increased electronegativity of *H then leads to a more final-statelike transition state, which increases the charge transfer coefficient and reduces the Tafel slope.

The defective MoS_2 is much more intrinsically active for HER than the pristine case. By increasing the gate voltage, we find a similar, almost linear reduction of the overpotential and a decrease of the Tafel slope as in the pristine case. Both the pristine and the defective systems can thus be activated to a comparable degree by applying the gate voltage. Additionally, the increased conductivity also helps to reduce the *iR* loss in electron transport in MoS_2 and between MoS_2 and current collector,[19] which contributes to the enhanced performance.

To demonstrate the reversibility and in situ tuning capability of our SIGMA method, a "catalysis transistor" was tested as shown in Figure 3c. The HER voltage between the working and reference electrodes was kept constant (V_{HER} = −0.2 V) and the gate voltage was swept from 0 to 3 V with a 10 mV/s step. This type of test is similar to the I_d−V_g transfer curve in a transistor to characterize the gate induced on/off states. For both the pristine and defective samples, the HER currents increase with the gate voltage, which makes it behave as an n-type channel transistor. The similar on/off ratio of ∼7 of the pristine and defective device is obtained, indicating a similar underlying mechanism which will be discussed later. The gating effect is reversible with hysteresis. The hysteresis of catalysis transistor is larger than that of the MoS_2−LaF_3 EDLT.[18] The enhanced hysteresis could result from the aqueous environment of the catalysis transistor. Previous researches have reported that water molecular phyisorbe on the MoS_2 surface facilitate positive charge trapping and detrapping at the trap levels.[33,34] Additionally, the hydrogen absorption and dissociation on the MoS_2 surface contribute to the hysteresis. The hysteresis makes the HER performance depends on the gate voltage sweep range, direction and rate, however, it can be also utilized to fabricate "catalysis memory" to store information by catalytic activities.

A comparison of our SIGMA method and other reported methods is presented in Figure 3d. Each existing methods give a point in the figure, whereas our SIGMA method shows a dynamic and continuously tunable range. The optimized performance of our method is close to the best performance from those sophisticated designs.

Tuning the gate voltage with SIGMA increases the charge carrier density, which can have a significant impact on surface electrocatalysis. In the case of HER, the overall reaction rate has been shown to be determined mainly by the *H binding energy, ΔG_{ads}.[23] A binding energy that is too weak ($\Delta G_{ads} > 0$) or too strong ($\Delta G_{ads} < 0$) will cause the rate to be limited by the *H adsorption (Volmer) step or desorption (Heyrovsky/Tafel) steps, respectively. A binding energy of $\Delta G_{ads} \approx 0$ has been determined as a characteristic of an ideal HER catalyst.[35] A previous study has shown that the basal plane should not be considered as an active site with 3% of S-vacancies already exhibiting orders of magnitude higher HER activity.[30] In our as-grown pristine MoS_2, a small ratio of intrinsic atomic defects is unavoidable.[36,37] Beside the sulfur vacancies, the hydrogen coverage (number of H atoms over number of S atoms on the

DOI: 10.1021/acs.nanolett.9b02888
Nano Lett. XXXX, XXX, XXX−XXX

upper side of MoS_2 unit cell) has been also shown to affect the activation barrier of the reaction.[38]

We evaluated ΔG_{ads} at varying sulfur vacancy coverages as a function of charge carrier density. Figure 4b shows the results of pristine (0%) and 13% sulfur vacancy MoS_2 under a hydrogen coverage of 16.7%. The results of different levels of defects and hydrogen coverages are presented in Figure S10. We found that the added negative surface charge stabilizes *H in all considered cases. This finding is consistent with previous studies, which found *H binding to be stabilized in the presence of excess electrons, thereby reducing the Volmer thermochemical reaction barrier.[19] Thermodynamically, at the applied HER voltages all vacancies can be expected to be covered with H atoms.[30] By introducing excess electrons into the system under a high hydrogen coverage and high vacancy density, we found ΔG_{ads} approach a value of zero under the range of experimentally estimated carrier densities. This minimization of the thermochemical H adsorption barrier that we see for most considered coverages is in agreement with the experimentally observed HER overpotential reduction. Furthermore, theory predicts a similar *H binding energy change with carrier density, independent of the vacancy coverage, in line with the experimental findings. We finally also comment on the stabilization of *H to negative ΔG_{ads} values with gate voltage that we observe in the case of small vacancy concentrations (4.2%), as shown in the Supporting Information. In this case, one would expect a decrease in the HER activity as gate voltage increases. This finding suggests that HER proceeds mainly from clustered S-vacancy regions, corresponding to higher local *H coverages and optimal binding energies under an applied gate voltage.

Additionally, in typical electrochemical devices, the surface charge of a catalyst affects the potential drop which drives charge-transfer kinetics at the solid−liquid interface (Frumkin effect). In the device considered here, the SIGMA-induced carrier density in MoS_2 is, however, fully compensated by the surface charge density of LaF_3 due to its comparably high capacitance. The electric field is thus completely screened and the potential driving force is nearly independent of the applied gate voltage. However, if the gate voltage is too high (>3 V), the field effect cannot be completely screened by the MoS_2 and will penetrate through the electrolyte.[39] The leaking field accumulates excessive electrons at the electrical double layer of solvent and MoS_2, thus affecting the electrochemical potential of reactive proton donors as well as the local pH at the outer Helmholtz layer.

Therefore, our catalysis transistor modulates the *H binding energy (ΔG_{ads}) by changing the carrier density of the catalyst through the electric field, which facially manifests as the modulation of catalytic current density. This technique can be used to control the activity of catalysts and integrated with existing circuit technology for a variety of applications. For example, in the on-demand fuel production or biomimetic systems it can be used as a key component in feedback loop to generate regulated TOF as needed dynamically.

Conclusion. In this work, we developed a new approach (SIGMA) to dynamically, continuously, and reversibly tune the catalytic performance of electrochemical devices. As for the MoS_2-catalyzed HER, our experimental and theoretical results show that SIGMA tunes the carrier density of MoS_2 up to 5×10^{13} cm^{-2}. These additional electrons drive the hydrogen adsorption energy to zero and increase the electronic conductivity of MoS_2. SIGMA tuning of surface charge density and electric fields could represent a general strategy to tune and improve the catalytic activity without modifying structure and composition of the catalysts. In addition to fundamental studies, the catalysis transistor makes it possible to integrate the electrochemical reactions with advanced circuit technology for various on-demand applications.

Methods. *CVD Growth and Transfer of Monolayer MoS_2.* Monolayer single crystal 2H-MoS_2 was grown in a tube furnace by CVD with molybdenum trioxide (MoO_3) and sulfur (S) powder as precursors and argon as the carrier gas. A Si substrate with 300 nm oxide layer was suspended face-down on a quartz boat containing the MoO_3 source. The growth process was conducted at 750 °C with 5 sccm Ar flow at atmospheric pressure and Ar environment. After 15 min growth, the furnace was cooled down to room temperature. The triangular single crystal was on the edges of the continuous film. To transfer the MoS_2, a layer of PMMA was first spin-coated (4000 rpm) and the sample was baked at 120 °C for 2 min. The diluted potassium hydroxide (KOH) solution was then used as the etchant to etch away the SiO_2 layer. After that, the PMMA/MoS_2 layer was lifted off and then transferred onto a LaF_3 substrate. Finally, the sample was air-dried and the PMMA was washed off with acetone and 2-propanol.

Generating Defective MoS_2. The argon plasma treatment was carried out by using an Oxford 80 reactive ion etcher with an 8 W power supply. The gas pressure was controlled at 900 mTorr by flowing argon at 100 sccm. The ∼13% S-vacancies could be achieved by ∼20 s exposure.

Device Fabrication. The electron beam lithography was conducted by a JBX-6300FS electron beam lithography system to pattern the electrodes. The metal evaporation process was done by a KJ Lesker e-gun/beam evaporator with a speed of 1 Å/s and a base pressure under 10^{-6} Torr.

Electrochemical Measurements. The electrochemical testing was performed using a three electrodes setup. A sharp carbon rod was used as a counter electrode, while a homemade Ag/AgCl reference electrode was used as a reference electrode. The reference voltage of the homemade Ag/AgCl was calibrated by standard hydrogen evolution. The MoS_2 flake was used as a working electrode. A drop (∼30 μL) of 0.5 M sulfuric acid (H_2SO_4) solution was used as the electrolyte. The LSV scan rate was 5 mV/s.

DFT Calculation. DFT calculations of reaction energetics were carried out with a periodic plane-wave implementation and ultrasoft pseudopotentials using QUANTUM ESPRESSO version 6.1[40] interfaced with the atomistic simulation environment (ASE).[41]

■ ASSOCIATED CONTENT

Supporting Information

The Supporting Information is available free of charge on the ACS Publications website at DOI: 10.1021/acs.nanolett.9b02888.

Figures S1−S10, additional text, additional references (PDF)

■ AUTHOR INFORMATION

Corresponding Authors

*(K.C.) E-mail: kchan@fysik.dtu.dk.
*(Y.C.) E-mail: yicui@stanford.edu.

ORCID

Yecun Wu: 0000-0001-6011-4489

DOI: 10.1021/acs.nanolett.9b02888
Nano Lett. XXXX, XXX, XXX−XXX

Chun-Lan Wu: 0000-0001-7124-1520
Wei Chen: 0000-0001-7701-1363
Ankun Yang: 0000-0002-0274-4025
Hao Chen: 0000-0002-2852-0070
Guangmin Zhou: 0000-0002-3629-5686
Karen Chan: 0000-0002-6897-1108
Yi Cui: 0000-0002-6103-6352

Author Contributions

Y.W. and Y.C. conceived the idea and designed the experiments. Y.W. performed material growth, electrode fabrication, and electrochemical measurements. S.R., M.T., and K.C. carried out the theoretical calculations. C.-L.W. and A.Y. assisted with the material growth, electrode fabrication, and characterization. W.C. assisted with the electrochemical measurements. H.C. performed the SEM and XPS measurement. Y.W., S. R., and Y.C. wrote the manuscript, and all authors discussed the results and commented on the manuscript.

Author Contributions

$^{\circ}$Y.W. and S. R. contributed equally to this work.

Notes

The authors declare no competing financial interest.

■ ACKNOWLEDGMENTS

This work was supported by the U.S. Department of Energy (DOE), Office of Basic Energy Sciences, Division of Materials Sciences and Engineering (Contract No. DE-AC02-76SF00515). Part of this work was performed at the Stanford Nano Shared Facilities (SNSF), supported by the National Science Foundation under award ECCS-1542152. Computational work was supported by the U.S. Department of Energy, Chemical Sciences, Geosciences, and Biosciences (CSGB) Division of the Office of Basic Energy Sciences, via Grant DE-AC02-76SF00515 to the SUNCAT Center for Interface Science and Catalysis. K.C. acknowledges a grant (9455) from the VILLUM FONDEN.

■ REFERENCES

(1) Seh, Z. W.; Kibsgaard, J.; Dickens, C. F.; Chorkendorff, I. B.; Norskov, J. K.; Jaramillo, T. F. *Science* **2017**, *355* (6321), eaad4998.
(2) Kong, D.; Cha, J. J.; Wang, H.; Lee, H.; Cui, Y. *Energy Environ. Sci.* **2013**, *6* (12), 3553−3558.
(3) Wang, H.; Tsai, C.; Kong, D.; Chan, K.; Abild-Pedersen, F.; Norskov, J.; Cui, Y. *Nano Res.* **2015**, *8* (2), 566−575.
(4) Zheng, X.; Ji, Y.; Tang, J.; Wang, J.; Liu, B.; Steinruck, H. G.; Lim, K.; Li, Y.; Toney, M. F.; Chan, K.; Cui, Y. *Nat. Catal.* **2019**, *2* (1), 55−61.
(5) Lu, Z.; Chen, G.; Li, Y.; Wang, H.; Xie, J.; Liao, L.; Liu, C.; Liu, Y.; Wu, T.; Li, Y.; Luntz, A. C.; Bajdich, M.; Cui, Y. *J. Am. Chem. Soc.* **2017**, *139* (17), 6270−6276.
(6) Ye, G.; Gong, Y.; Lin, J.; Li, B.; He, Y.; Pantelides, S. T.; Zhou, W.; Vajtai, R.; Ajayan, P. M. *Nano Lett.* **2016**, *16* (2), 1097−1103.
(7) Li, H.; Tsai, C.; Koh, A. L.; Cai, L.; Contryman, A. W.; Fragapane, A. H.; Zhao, J.; Han, H.; Manoharan, H. C.; Abild-Pedersen, F.; Norskov, J. K.; Zheng, X. *Nat. Mater.* **2016**, *15* (3), 364.
(8) Lu, Z.; Jiang, K.; Chen, G.; Wang, H.; Cui, Y. *Adv. Mater.* **2018**, *30* (48), 1800978.
(9) Wang, H.; Xu, S.; Tsai, C.; Li, Y.; Liu, C.; Zhao, J.; Liu, Y.; Yuan, H.; Abild-Pedersen, F.; Prinz, F. B.; Norskov, J. K.; Cui, Y. *Science* **2016**, *354* (6315), 1031−1036.
(10) Wang, L.; Zeng, Z. H.; Gao, W. P.; Maxson, T.; Raciti, D.; Giroux, M.; Pan, X. Q.; Wang, C.; Greeley, J. *Science* **2019**, *363* (6429), 870.
(11) Radisavljevic, B.; Radenovic, A.; Brivio, J.; Giacometti, V.; Kis, A. *Nat. Nanotechnol.* **2011**, *6* (3), 147−150.
(12) Liu, Y.; Duan, X.; Huang, Y.; Duan, X. *Chem. Soc. Rev.* **2018**, *47* (16), 6388−6409.
(13) Mak, K. F.; Shan, J. *Nat. Photonics* **2016**, *10* (4), 216−226.
(14) Sood, A.; Xiong, F.; Chen, S.; Wang, H.; Selli, D.; Zhang, J.; McClellan, C. J.; Sun, J.; Donadio, D.; Cui, Y.; Pop, E.; Goodson, K. E. *Nat. Commun.* **2018**, *9*, 4510.
(15) Wang, J.; Yan, M.; Zhao, K.; Liao, X.; Wang, P.; Pan, X.; Yang, W.; Mai, L. *Adv. Mater.* **2017**, *29* (7), 1604464.
(16) Deng, Y.; Yu, Y.; Song, Y.; Zhang, J.; Wang, N. Z.; Sun, Z.; Yi, Y.; Wu, Y. Z.; Wu, S.; Zhu, J.; Wang, J.; Chen, X. H.; Zhang, Y. *Nature* **2018**, *563* (7729), 94−99.
(17) Zhang, Y.; Ye, J.; Matsuhashi, Y.; Iwasa, Y. *Nano Lett.* **2012**, *12* (3), 1136−40.
(18) Wu, C.-L.; Yuan, H.; Li, Y.; Gong, Y.; Hwang, H. Y.; Cui, Y. *Nano Lett.* **2018**, *18* (4), 2387−2392.
(19) Voiry, D.; Fullon, R.; Yang, J.; Silva, C. D. C. E.; Kappera, R.; Bozkurt, I.; Kaplan, D.; Lagos, M. J.; Batson, P. E.; Gupta, G.; Mohite, A. D.; Dong, L.; Er, D.; Shenoy, V. B.; Asefa, T.; Chhowalla, M. *Nat. Mater.* **2016**, *15* (9), 1003−1009.
(20) Ding, Q.; Song, B.; Xu, P.; Jin, S. *Chem.* **2016**, *1* (5), 699−726.
(21) Deng, D.; Novoselov, K. S.; Fu, Q.; Zheng, N.; Tian, Z.; Bao, X. *Nat. Nanotechnol.* **2016**, *11* (3), 218−230.
(22) Desai, S. B.; Madhvapathy, S. R.; Sachid, A. B.; Llinas, J. P.; Wang, Q.; Ahn, G. H.; Pitner, G.; Kim, M. J.; Bokor, J.; Hu, C.; Wong, H.-S. P.; Javey, A. *Science* **2016**, *354* (6308), 99−102.
(23) Jaramillo, T. F.; Jorgensen, K. P.; Bonde, J.; Nielsen, J. H.; Horch, S.; Chorkendorff, I. *Science* **2007**, *317* (5834), 100−102.
(24) Zhang, J.; Wu, J.; Guo, H.; Chen, W.; Yuan, J.; Martinez, U.; Gupta, G.; Mohite, A.; Ajayan, P. M.; Lou, J. *Adv. Mater.* **2017**, *29* (42), 1701955.
(25) Sun, Y.; Gao, S.; Lei, F.; Xie, Y. *Chem. Soc. Rev.* **2015**, *44* (3), 623−636.
(26) Kong, D.; Wang, H.; Cha, J.; Pasta, M.; Koski, K. J.; Yao, J.; Cui, Y. *Nano Lett.* **2013**, *13* (3), 1341−1347.
(27) Kibsgaard, J.; Chen, Z.; Reinecke, B. N.; Jaramillo, T. F. *Nat. Mater.* **2012**, *11* (11), 963−969.
(28) Wang, H.; Lu, Z.; Xu, S.; Kong, D.; Cha, J. J.; Zheng, G.; Hsu, P.-C.; Yan, K.; Bradshaw, D.; Prinz, F. B.; Cui, Y. *Proc. Natl. Acad. Sci. U. S. A.* **2013**, *110* (49), 19701−19706.
(29) Luo, Z.; Ouyang, Y.; Zhang, H.; Xiao, M.; Ge, J.; Jiang, Z.; Wang, J.; Tang, D.; Cao, X.; Liu, C.; Xing, W. *Nat. Commun.* **2018**, *9*, 2120.
(30) Tsai, C.; Li, H.; Park, S.; Park, J.; Han, H.; Norskov, J. K.; Zheng, X.; Abild-Pedersen, F. *Nat. Commun.* **2017**, *8*, 15113.
(31) Leong, W. S.; Li, Y.; Luo, X.; Nai, C. T.; Quek, S. Y.; Thong, J. T. L. *Nanoscale* **2015**, *7* (24), 10823−10831.
(32) Bader, R. F. W. *Atoms in molecules: a quantum theory*; Clarendon Press: Oxford, 1990.
(33) Late, D. J.; Liu, B.; Matte, H. S. S. R.; Dravid, V. P.; Rao, C. N. R. *ACS Nano* **2012**, *6* (6), 5635−5641.
(34) Di Bartolomeo, A.; Genovese, L.; Giubileo, F.; Iemmo, L.; Luongo, G.; Foller, T.; Schleberger, M. *2D Mater.* **2018**, *5* (1), 015014.
(35) Norskov, J. K.; Bligaard, T.; Logadottir, A.; Kitchin, J. R.; Chen, J. G.; Pandelov, S.; Norskov, J. K. *J. Electrochem. Soc.* **2005**, *152* (3), J23−J26.
(36) Hong, J.; Hu, Z.; Probert, M.; Li, K.; Lv, D.; Yang, X.; Gu, L.; Mao, N.; Feng, Q.; Xie, L.; Zhang, J.; Wu, D.; Zhang, Z.; Jin, C.; Ji, W.; Zhang, X.; Yuan, J.; Zhang, Z. *Nat. Commun.* **2015**, *6*, 6293.
(37) Zhou, W.; Zou, X.; Najmaei, S.; Liu, Z.; Shi, Y.; Kong, J.; Lou, J.; Ajayan, P. M.; Yakobson, B. I.; Idrobo, J. C. *Nano Lett.* **2013**, *13* (6), 2615−2622.
(38) Skulason, E.; Tripkovic, V.; Bjorketun, M. E.; Gudmundsdottir, S.; Karlberg, G.; Rossmeisl, J.; Bligaard, T.; Jonsson, H.; Norskov, J. K. *J. Phys. Chem. C* **2010**, *114* (50), 22374−22374.
(39) Castellanos-Gomez, A.; Cappelluti, E.; Roldan, R.; Agrait, N.; Guinea, F.; Rubio-Bollinger, G. *Adv. Mater.* **2013**, *25* (6), 899−903.

DOI: 10.1021/acs.nanolett.9b02888
Nano Lett. XXXX, XXX, XXX−XXX

(40) Giannozzi, P.; Baroni, S.; Bonini, N.; Calandra, M.; Car, R.; Cavazzoni, C.; Ceresoli, D.; Chiarotti, G. L.; Cococcioni, M.; Dabo, I.; Dal Corso, A.; de Gironcoli, S.; Fabris, S.; Fratesi, G.; Gebauer, R.; Gerstmann, U.; Gougoussis, C.; Kokalj, A.; Lazzeri, M.; Martin-Samos, L.; Marzari, N.; Mauri, F.; Mazzarello, R.; Paolini, S.; Pasquarello, A.; Paulatto, L.; Sbraccia, C.; Scandolo, S.; Sclauzero, G.; Seitsonen, A. P.; Smogunov, A.; Umari, P.; Wentzcovitch, R. M. *J. Phys.: Condens. Matter* **2009**, *21* (39), 395502.
(41) Larsen, A. H.; Mortensen, J. J.; Blomqvist, J.; Castelli, I. E.; Christensen, R.; Dulak, M.; Friis, J.; Groves, M. N.; Hammer, B.; Hargus, C.; Hermes, E. D.; Jennings, P. C.; Jensen, P. B.; Kermode, J.; Kitchin, J. R.; Kolsbjerg, E. L.; Kubal, J.; Kaasbjerg, K.; Lysgaard, S.; Maronsson, J. B.; Maxson, T.; Olsen, T.; Pastewka, L.; Peterson, A.; Rostgaard, C.; Schiotz, J.; Schutt, O.; Strange, M.; Thygesen, K. S.; Vegge, T.; Vilhelmsen, L.; Walter, M.; Zeng, Z. H.; Jacobsen, K. W. *J. Phys.: Condens. Matter* **2017**, *29* (27), 273002.

DOI: 10.1021/acs.nanolett.9b02888
Nano Lett. XXXX, XXX, XXX−XXX